DOI: 10.1002/ejic.201001218

Substrate Hydroxylation by the Oxido–Iron Intermediate in Aromatic Amino Acid Hydroxylases: A DFT Mechanistic Study

Elaine Olsson,[a] Aurora Martinez,[b] Knut Teigen,[b] and Vidar R. Jensen*[a]

Keywords: Amino acids / Hydroxylation / 5,6,7,8-Tetrahydrobiopterin / Density functional calculations / Iron

Substrate hydroxylation by an Fe^{IV}=O cluster model of the active center in aromatic amino acid hydroxylases (AAHs) has been investigated by means of DFT calculations. Whereas benzene was used as a model for the aromatic amino acid substrate, the water-free Fe^{IV}=O cluster model has been used in previous studies of enzyme activation and formation of the hydroxylating intermediate. This cluster model also has the pterin cofactor placed in the first coordination sphere of the iron atom and differs substantially from models used in previous computational studies of AAH-catalyzed hydroxylations. The formation of the (Fe)O–C-(benzene) bond is associated with a free-energy barrier (12.6 kcal mol^{-1}) that is slightly lower than that calculated previously for the formation of the Fe^{IV}=O species. The subsequent steps, the NIH shift and the tautomerization leading to the phenol product are both associated with lower energy barriers. The substrate hydroxylation is followed by protonation of the oxidized iron-bound cofactor to give the pterin-4a-carbinolamine product. The latter is subsequently dissociated upon rebinding of water molecules to produce the hexacoordinate iron complex of the enzyme resting state. Consequently, no product is released before the oxidation of both the substrate and the cofactor has been completed. Finally, the current study completes the catalytic cycle and regenerates the catalyst, with a barrier energy comparable to that of the (Fe)O–C(benzene) bond formation.

Introduction

The aromatic amino acid hydroxylases (AAHs) constitute a family of enzymes including phenylalanine hydroxylase (PAH), tyrosine hydroxylase (TH), and the tryptophan hydroxylases (TPHs) that catalyze the hydroxylation of aromatic amino acids.[1–6] PAH catalyzes the conversion of L-phenylalanine (L-Phe) to L-tyrosine (L-Tyr) mainly in the liver. TH catalyzes the hydroxylation of L-Tyr to L-dihydroxyphenylalanine (L-Dopa) in the brain and neuroendocrine tissues, and TPH1 and TPH2 convert L-tryptophan (L-Trp) to 5-hydroxytryptophan, also in the nervous system.[3,7] The AAHs are non-heme iron enzymes that are dependent on the cofactor (6*R*)-L-erythro-5,6,7,8-tetrahydrobiopterin (BH_4) and use dioxygen as an additional substrate (Scheme 1). The pterin cofactor activates the iron atom by reducing it from the ferric to the ferrous form, in a step prior to catalysis, and during the catalytic cycle BH_4 is oxidized to pterin-4a-carbinolamine (4a-HO–BH_4) (Scheme 2). The dioxygen atoms are incorporated both into the substrate and the pterin cofactor.[8–13]

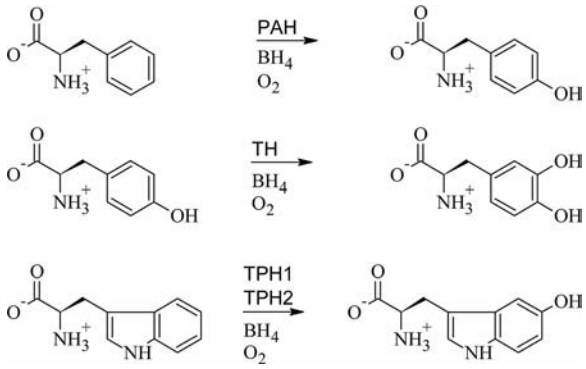

Scheme 1. Hydroxylation of the aromatic amino acids L-Phe, L-Tyr, and L-Trp by their respective hydroxylases, phenylalanine hydroxylase (PAH), tyrosine hydroxylase (TH), and tryptophan hydroxylase 1 and 2 (TPH1 and TPH2). The hydroxylases use the cofactor BH_4 and O_2 as additional substrates in the reaction.

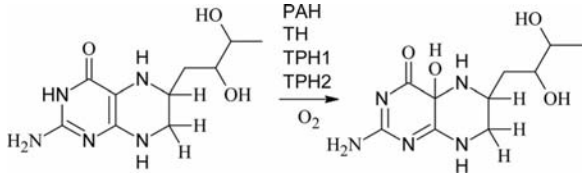

Scheme 2. Cofactor (6*R*)-L-erythro-5,6,7,8-tetrahydrobiopterin (BH_4) is oxidized to pterin-4a-carbinolamine (4a-HO–BH_4) by the AAHs.

[a] Department of Chemistry, University of Bergen, Allégaten 41, 5007 Bergen, Norway
Fax: +47-55589490
E-mail: Vidar.Jensen@kj.uib.no
[b] Department of Biomedicine, University of Bergen, Jonas Lies vei 91, 5009, Bergen, Norway

Supporting information for this article is available on the WWW under http://dx.doi.org/10.1002/ejic.201001218.

Mammalian AAHs consist of a regulatory, a catalytic, and an oligomerization domain. The catalytic domain includes the active site iron, where it is anchored by two histidines (His) and one glutamic acid (Glu).[1,4] X-ray crystal structures of the AAHs in binary complexes with the cofactor or cofactor analogue, have in addition to the 2-His–1-Glu binding motif, three or two ligating water molecules (Figure 1).[14–16] The water molecules all seem to dissociate upon binding of substrate and cofactor, leading to a ternary complex, prior to the formation of the active quaternary (e.g. PAH–Fe^{II}–BH_4–L-Phe–O_2 in the case of PAH) complex. In a DFT investigation we have recently shown that the formation of the active water-free O_2 complex from the initial water-ligated structure is facile.[17]

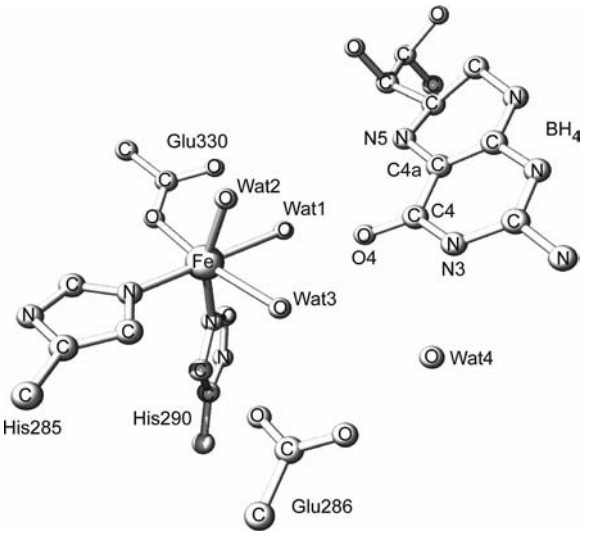

Figure 1. Active site in the X-ray crystal structure of the catalytic domain of human PAH in a binary complex with the pterin cofactor (PDBid: 1J8U).[14] The iron atom is ligated by the 2-His–1-Glu binding motif and three water molecules.

Because of the high sequence similarity within the catalytic domains of the AAHs, it is widely assumed that the hydroxylation reaction mechanism is similar for the three enzymes.[2–4,18] Moreover, it is also assumed that this general AAH reaction mechanism follows a two-step reaction route where an oxido–iron species is formed in the first step after cleavage of the O–O bond in an Fe–O–O–BH_4 bridge. Next, the Fe^{IV}=O species is responsible for the hydroxylation of the substrate in the second step.[19–21] A high-spin Fe^{IV} species has been directly observed in TH using Mössbauer and electron paramagnetic resonance spectroscopy, and has been associated with the Fe^{IV}=O hydroxylating intermediate.[22] Mechanistic DFT investigations on the formation of Fe^{IV}=O, using gas-phase cluster models,[23–24] have arrived at two different rate-limiting steps for the formation of the Fe^{IV}=O complex. Whereas, in the study of Bassan et al.,[23] the formation of the Fe–O–O–BH_4 bridge was found to be rate-limiting, in our recent study of the formation of the Fe^{IV}=O species, this role was associated with an earlier step, a one-electron transfer from the cofactor to dioxygen, which initiates the reduction of the latter.[24] An early rate-limiting step involving such a one-electron transfer has been proposed based on measurements of ^{18}O kinetic isotope effects.[25] It has subsequently also been reported that the second main step, the hydroxylation of the aromatic substrate (see below), more specifically the incorporation of the oxygen into the substrate, could, completely or partially, be rate-limiting.[26,27]

In the second main reaction step, the aromatic amino acid substrate is hydroxylated by Fe^{IV}=O through an attack by the carbon atom in the aromatic ring on the oxygen atom in Fe^{IV}=O, followed by a subsequent 1,2-hydride transfer, a so-called NIH shift, to form a dienone.[28–30] Organic catalysts are not able to perform NIH shifts, and even the low-yield nonspecific hydroxylation of L-Phe by BH_4 in the absence of enzyme occurs without an NIH shift.[31] This NIH shift has been considered as evidence for an arene oxide formation,[32] and as a final step, a tautomerization of the ketone to the phenol form completes the formation of the amino acid product. It is known that no product (oxidized amino acid or oxidized cofactor) is released before all substrates i.e. amino acid substrate, BH_4, and O_2 have been bound to the active site, although the order of the binding is not completely established.[3,32] Steady-state kinetics on rat TH and bacterial PAH suggest a binding order of cofactor, substrate, and O_2.[26,33] Fitzpatrick showed, by using kinetic isotope effects, that the rate of hydroxylation of Phe by TH in the 4-position was independent of the rate of hydroxylation in the 3- or 5-position, and concluded that the hydroxylation did not proceed via an arene oxide intermediate.[29] Furthermore, Hillas et al. showed that the intermediate for the hydroxylation of the substrate was electron-deficient and proposed a cationic intermediate.[34] DFT studies, in which the hydroxylation of the substrate by the Fe^{IV}=O species has been investigated, are also not commensurate with the formation of an arene oxide intermediate.[35,36] In these studies, two different models have been used, one in which a water molecule and a hydroxy group are coordinated to the iron atom in addition to the 2-His–1-Glu triad (HO–Fe^{IV}=O), and the other in which the hydroxy group was protonated [H_2O–Fe^{IV}=O]$^+$. The investigations of the HO–Fe^{IV}=O complex supported a two-step oxidation for the formation of the C–O bond, with an unpaired electron located in the benzene ring after the first step.[35] The model with the protonated hydroxy group predicted the formation of an arenium cation.[35,36] The [H_2O–Fe^{IV}=O]$^+$ model was taken to be the QM part in a QM/MM investigation. The QM geometry was seen to change only little upon inclusion of the surrounding protein in the QM/MM investigation.[36]

In the present work we have investigated the hydroxylation of the aromatic amino acid substrate by the Fe^{IV}=O hydroxylating intermediate. The starting structure (**12a**, Figure 2) is the gas-phase cluster model of the water-free Fe^{IV}=O species arrived at in the recent study of the first part of the reaction mechanism of the AAHs.[24] In the present study we move on to investigate the details of the Fe^{IV}=O-catalyzed substrate hydroxylation in AAHs using a water-free model containing the cofactor in the first coordi-

nation sphere. In the end, the hexacoordinate iron complex is regenerated by rebinding the three water molecules that were dissociated prior to dioxygen binding.

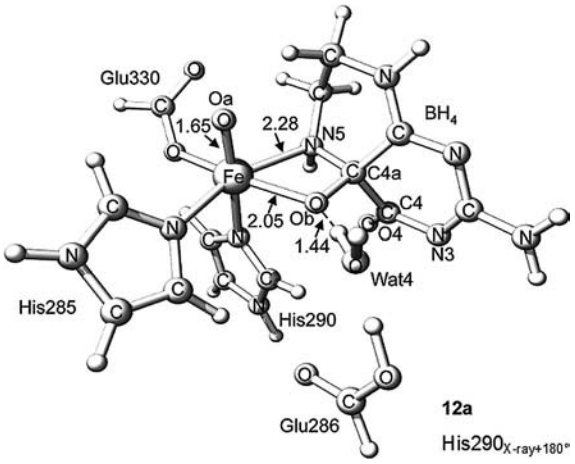

Figure 2. Geometry-optimized Fe^{IV}=O intermediate, which constitutes the starting point in the present study and which was arrived at in the preceding DFT study on formation of this intermediate.[24] Distances are given in Å.

In order to reduce the total structural model size, benzene was selected in the present study as a simplified model for L-Phe. This appears as an appropriate substrate model for all AAHs. Thus, although the AAHs are substrate-specific, and this specificity is defined by the structure of the catalytic domain and modulated by the regulatory domain,[6] only TH can hydroxylate L-Tyr, whereas all three AAHs can hydroxylate L-Phe.[2,6]

Results and Discussion

The structure constituting the starting point of the present investigation (**12a**) was arrived at in the previous DFT study of the formation of the hydroxylating oxido–iron intermediate.[24] The original gas-phase cluster model, employed in the initial study of water dissociation and dioxygen binding,[17] was derived from the X-ray crystal structure of the catalytic domain of human (h) PAH in a binary complex with the cofactor tetrahydrobiopterin (hPAH–Fe^{II}–BH_4, PDBid: 1J8U).[14] The non-heme iron atom with two His (His285 and His290), Glu (Glu330), and three water molecules [H_2O-1250 (Wat1), H_2O-1251 (Wat2) and H_2O-1253 (Wat3)] was extracted from the X-ray crystal structure. Also included in the model were the cofactors Glu286 and H_2O-1142 (Wat4), all found in the second coordination sphere of the iron atom in the X-ray crystal structure (Figure 1). Imidazole was used to model His, and Glu was modeled by formate. The dihydroxypropyl chain at C6 of the cofactor was substituted by a hydrogen atom. The present study also involves the amino acid substrate, which, as in previous studies,[35,37] is modeled by benzene. The Fe^{IV}=O complex (**12a**) is hexacoordinate with the cofactor placed in the first coordination sphere of the iron atom, coordinating in a bidentate fashion through the atoms Ob (2.05 Å) and N5 (2.28 Å) (cf. Figure 2).

Hydroxylation of the Aromatic Substrate

Up to this point in the reaction, benzene appears to interact only very weakly with the iron complex. A series of tests were performed in which benzene was added to the structures **7a**, **8b**, **9a**, **9b**, and **12a** of the earlier investigations[17,24] and allowed to relax in various conformations. In all cases the obtained bond enthalpy to benzene was below 2.5 kcal mol^{-1}, and the atoms in the iron complexes in the respective structure pairs, with and without benzene, could be superimposed[38] with small weighted root mean square (RMS) deviations (0.07–0.17 Å; see Figure S1 in the Supporting Information). Benzene has therefore only been introduced in the current investigation of the aromatic substrate hydroxylation. Benzene was omitted from the models used in the previous DFT investigations of dioxygen binding and activation and formation of the Fe^{IV}=O intermediate, despite the fact that the substrate would also be present during the initial steps leading to water release and formation of the hydroxylating species.[17,24]

The free-energy cost of binding benzene to **12a**, to give **13a** (Figure 3), is close to 5 kcal mol^{-1}, with the closest benzene carbon atom located 3.42 Å from O(=Fe). Because of the lack of surrounding protein in the present cluster model, there is no substrate-guiding pocket. Moreover, a model substrate is used and substrate interactions with nearby residues are neglected. It is thus reasonable to believe that the cost of binding the substrate is exaggerated by the current model. Moreover, substrate binding takes place prior to, and triggers, loss of ligating water in the enzyme-activation phase,[39–43] and the free energy change associated with substrate binding should not be accounted for in

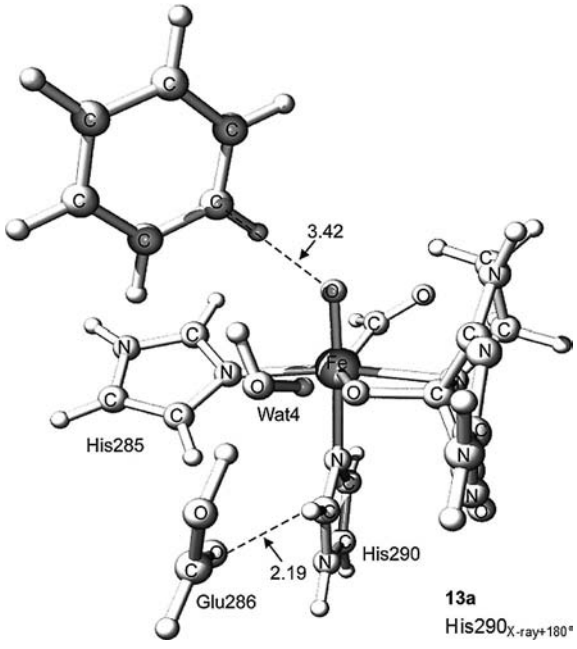

Figure 3. Geometry-optimized structure of the Fe^{IV}=O intermediate including benzene. The imidazole ring in His290 is rotated 180° relative to the conformation of the X-ray crystal structure (**$H290_{X\text{-}ray+180°}$**). Distances are given in Å.

the middle of the catalytic reaction. Unless otherwise stated, free energies are thus reported relative to **13a** (Figure 3) in the rest of this work. The lack of an active-site pocket and attractive substrate–pocket interactions also mean that there is no clear preference with regard to orientation of the benzene substrate. A number of different conformations were investigated, the most stable of which is that of **13a**. Although it is likely that the current cluster model and benzene substrate exaggerate the flexibility of the latter, considerable variations in position and orientation can also be seen for L-phenylalanine in a QM/MM study of PAH,[36] suggesting that the active-site pocket is indeed spacious and allows for a rather flexible substrate.

Another conformational flexibility pertaining to the imidazole ring in His290 was noted in our recent DFT investigations.[17,24] Conformations in which this ring was rotated 180° compared with that of the X-ray crystal structure were found to be of comparable, and sometimes lower, energy than that of the X-ray crystal structure conformation. For the oxido–iron complex including benzene (**13**), the conformer with the imidazole ring in His290 rotated 180° compared with that of the crystal structure (i.e. $\mathbf{H290_{X\text{-}ray+180°}}$; **13a**) is 1.6 kcal mol^{-1} (Table S2 in the Supporting Information and Figure 4) more stable than the conformer with the rotation as in the crystal structure (i.e. $\mathbf{H290_{X\text{-}ray}}$; **13b**, cf. Table S2 the Supporting Information). Thus, both conformers were systematically monitored throughout the reaction pathway, and the calculated free-energy difference between them never exceeds 2 kcal mol^{-1} (Figure 4). The lowest-energy conformation of each intermediate is given the suffix "**a**" whereas the second lowest conformation is termed "**b**". The present discussion is as much as possible restricted to the lowest-energy conformation ("**a**") in each case.

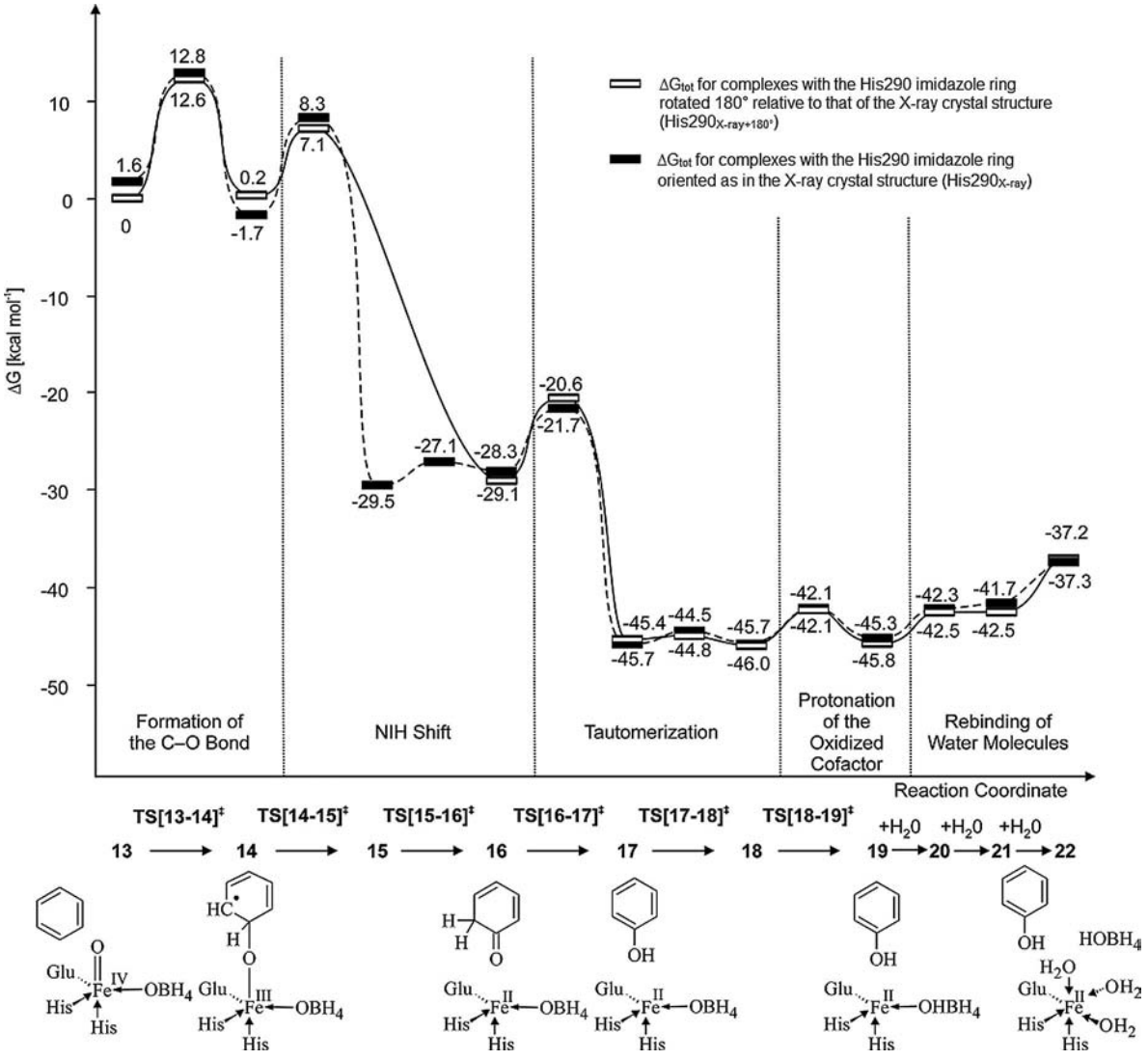

Figure 4. Calculated relative free energies [kcal mol^{-1}] for hydroxylation of the amino acid substrate by the Fe^{IV}=O species in AAHs. Energies are given relative to **13a**. For the conformer with the His290 imidazole ring rotated compared with that of the X-ray crystal structure, the rotation of Glu330 occurs simultaneously with the NIH shift, meaning that the reaction proceeds directly from **14b** to **16a**. Starting from **14a**, with the imidazole ring in His290 oriented as in the X-ray crystal structure. ($\mathbf{H290_{X\text{-}ray}}$), the NIH shift, leading to **15a**, and the rotation of Glu330, leading to **16b** via **TS[15a–16b]**‡, take place in separate steps.

Formation of the C–O Bond

The free-energy barrier associated with formation of the Oa–C(benzene) bond from **13a** is 12.6 kcal mol^{-1}. In the transition state (**TS[13a–14b]**‡, Figure 5), the reacting benzene carbon atom is located at a distance of 1.99 Å from Oa, and benzene approaches the oxygen atom in an end-on fashion. Attempts in which benzene was placed near the oxygen atom in a side-on fashion resulted in the rotation of the benzene ring and relaxation to the end-on structure. These observations are in line with the findings of Fitzpatrick, who, based on measurements of kinetic isotope effects, concluded that the formation of an arene epoxide intermediate is unlikely.[29]

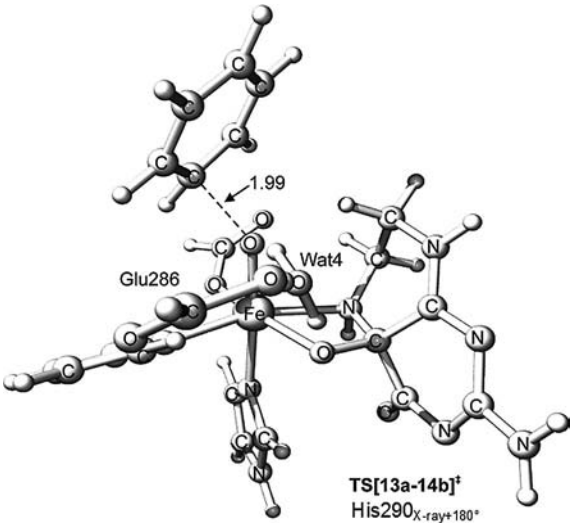

Figure 5. Optimized transition state for the formation of the (Fe)O–C(benzene) bond. Distances are given in Å.

Binding of benzene to the oxygen atom in **13b** to give **14a** is an exothermic as well as exergonic process (ΔH_{tot} = –5.0 kcal mol^{-1}, ΔG_{tot} = –3.3 kcal mol^{-1}). During the process of binding benzene to O(=Fe), Glu286 and Wat4 approach the substrate in a concerted way, remaining hydrogen-bonded to each other, which results in the rupture of the hydrogen bond between Glu286 and His290 present in **13a** and **13b**. The loss of the latter hydrogen bond is compensated for by the formation of a hydrogen bond between Wat4 and Oa(Fe) (bond length of 1.85 Å). The latter hydrogen bond also stabilizes the growing negative charge on Oa [q(Oa) = –0.93 e; cf. Table S3 in the Supporting Information]. It may be that the flexibility of Glu286, which here is seen to approach the substrate (compare structures **13a** and **14a**), is exaggerated by the current cluster model. Whether this is the case can only be clarified by a future QM/MM study including the protein environment. In such a study it would be possible to interpret deviations from the present reaction mechanism and reaction profile in terms of reduced residue flexibility compared with that of the present cluster model.

Upon going from **13b** to **14a**, the Oa–C(benzene) distance is drastically reduced and approaches that of a carbon–oxygen single bond in **14a**. This is corroborated by the corresponding Wiberg bond-order index (0.85; Table S4 in the Supporting Information) calculated for **14a**. Similarly, the Fe–Oa distance and the Wiberg bond-order index for **13b** and **14a** show that this bond is significantly weakened in the process. The O–benzene species (**14a**) carries an unpaired electron that is antiferromagnetically coupled to the unpaired electrons on the iron atom and its ligands. The unpaired electron on benzene is delocalized, with significant spin populations on the carbon atoms *ortho* (–0.38 and –0.38) and *para* (–0.49) relative to the recently oxidized carbon atom (see Figure 6 and Table S5 in the Supporting Information). The iron atom has now been reduced from Fe^{IV} to Fe^{III} (Scheme 3). The two-electron oxidation of benzene takes place over two steps, the first one-electron transfer from benzene to iron resulting in structure **14a**. The second electron transfer occurs early in the subsequent 1,2-hydride shift, in which a hydride on the oxidized ring carbon atom is transferred to an adjacent carbon atom (structure **15a**, Figure 7). In the transition state (**TS[14a–15a]**‡, Figure 8), no spin population is located on the O–benzene fragment, implying that the second electron transfer has already occurred (Table S5 in the Supporting Information and Scheme 3).

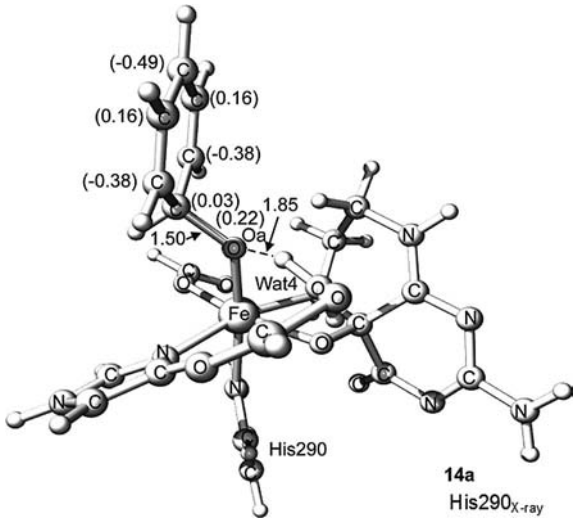

Figure 6. Geometry-optimized structure of the Fe^{IV}=O–benzene complex (Oa–C 1.50 Å). The spin populations on the carbon atoms and the inserted oxygen atom are shown in parentheses. Distances are given in Å.

QM and QM/MM calculations have previously shown C–O bond formation through direct electrophilic aromatic addition, as followed in this work, to be energetically preferable to a mechanism starting from C–H bond cleavage on the substrate.[36] Interestingly, calculations in which cationic models for the Fe^{IV}=O hydroxylating intermediate have been employed, have resulted in one-step two-electron oxidations of the substrate, leading to arenium ion intermediates,[35,36] whereas a mechanism involving two consecutive one-electron oxidations has been obtained for an overall neutral model, with a free energy barrier of 16.2 kcal mol^{-1} (using B3LYP).[35] Our results, obtained for a neutral model, agree with the latter study not only for the involve-

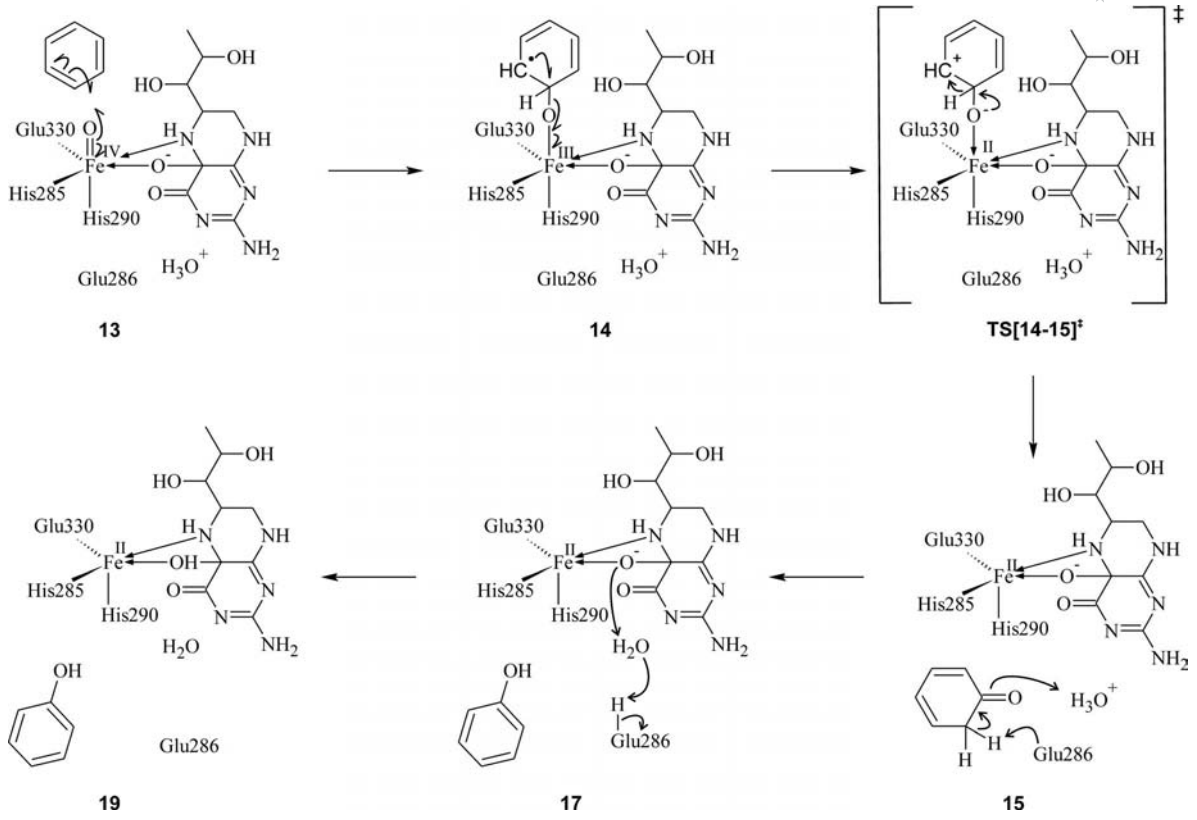

Scheme 3. The main electronic rearrangements as emerging from the calculations of the (Fe)O–C(benzene) bond formation, NIH shift, tautomerization and protonation of the oxidized cofactor.

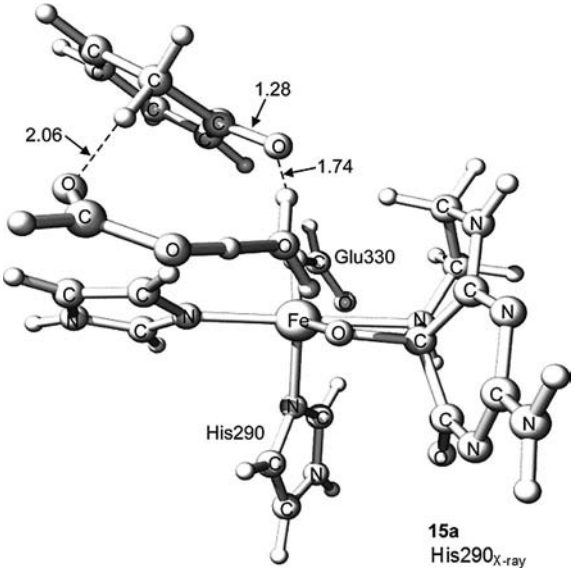

Figure 7. Geometry-optimized dienone resulting from the NIH shift. The substrate has dissociated from the iron atom. Distances are given in Å.

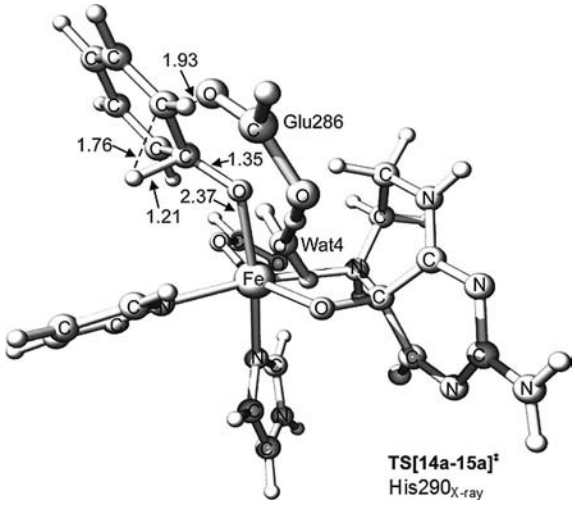

Figure 8. Optimized transition state for the NIH shift involving migration of the hydride on the oxidized carbon atom in the benzene ring to an adjacent carbon atom. Distances are given in Å.

ment of single-electron transfers. The calculated barrier energy ($\Delta G^{\ddagger}_{\text{tot-disp}}$ = 15.7 kcal mol^{-1}, i.e. excluding dispersion for comparison with ref.[35], $\Delta G^{\ddagger}_{\text{tot}}$ = 12.6 kcal mol^{-1}) is also similar when results from similar methods and basis sets are compared.

NIH Shift

The formation of the dienone, 2,4-cyclohexadiene intermediate (structure **15a**, Figure 7) involves a 1,2-hydride shift (NIH shift) in which the hydrogen atom on the oxidized benzene carbon atom migrates as a hydride to an adjacent carbon atom.

Because of the prospect of facilitating the subsequent tautomerization of the 2,4-cyclohexadiene through intermolecular proton transfers, the carbon atom close to Glu286 and Wat4 was chosen as the recipient in the NIH shift. The free-energy barrier for the NIH shift is calculated to be 10.0 kcal mol^{-1} (see **TS[14a–15a]**‡, Figure 8). The reaction **14a** → **15a** is exergonic by 27.8 kcal mol^{-1} and leaves the oxidized substrate in the second coordination sphere of the iron atom. Hydrogen bonds can be observed between Glu286 and one of the ketone hydrogen atoms as well as between the ketone oxygen atom and the hydronium ion (the protonated Wat4), the latter being particularly strong (1.74 Å). The position of the substrate thus prepares the latter for the tautomerization to be mediated by Glu286 and Wat4. In the most stable conformer (**15a**), the newly migrated hydrogen atom interacts with Glu286.

A facile rotation of Glu330 (see Figure 9) prepares for the tautomerization of the ketone to the phenol. This rotation changes the hydrogen-bond pattern directly by rupturing hydrogen bonds between Glu330 and the cofactor, on the one hand, and by establishing an analogous bond to His285, on the other hand. However, the rotation also affects hydrogen bonds in the region around the substrate, by, e.g., shortening the Wat4–O(benzene) hydrogen bond from 1.74 Å in **15a** to 1.60 Å in **16b** (both these structures are given in the Supporting Information), thus preparing for the proton transfer from Wat4 to the substrate. The transition state, **TS[15a–16b]**‡, for the rotation of Glu330 is shown in Figure 10. It should be noted that no product of tautomerization (**17**) without this rotated Glu330 conformation could be obtained in the calculations. In structure **16a**, the hydrogen bond from the ketone to Glu286 involves the hydrogen atom bound to the *ortho*-carbon atom prior to the NIH shift. Conformers in which the hydrogen bond to Glu286 involves the newly migrated (in the NIH shift) hydrogen atom have been found to be of competing stability (within ca. 1 kcal mol^{-1} less stable than **16a**, see the Supporting Information). This result indicates that both hydrogen atoms on the sp^3-hybridized carbon atom can be lost in the tautomerization, in agreement with results from the oral L-[$^2H_5$]Phe loading test in combination with mass spectrometry performed by Lehmann et al.[44] They concluded that the hydroxylation of Phe by PAH involved an NIH shift, followed by random loss of one of the hydrogen atoms at the sp^3-hybridized carbon atom.

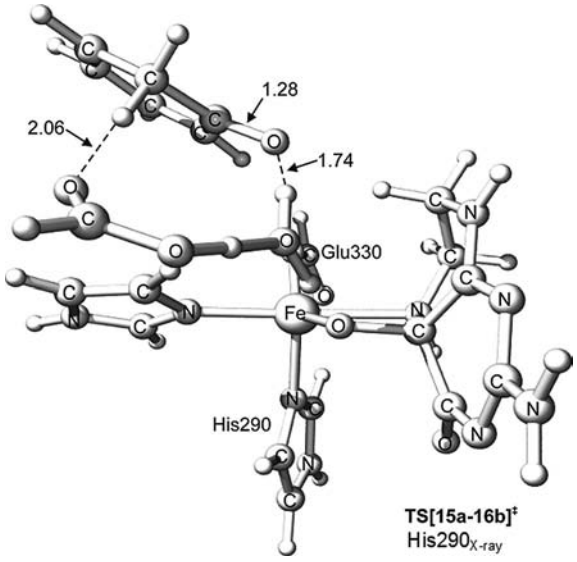

Figure 10. Geometry-optimized transition state for the rotation of Glu330. Distances are given in Å.

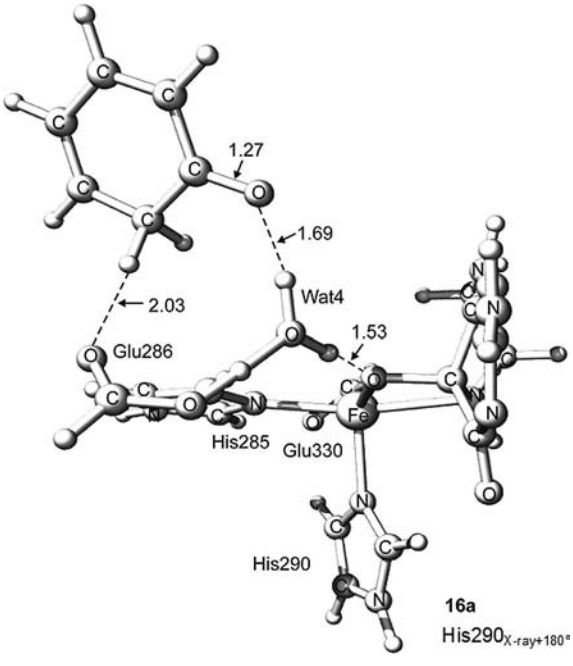

Figure 9. Geometry-optimized structure with rotated Glu330. Distances are given in Å.

Tautomerization

The final step in the transformation of the substrate product is the tautomerization from ketone to phenol. Two proton transfers occur simultaneously; from the sp^3-carbon atom of the ketone to Glu286 and from H_3O^+ (Wat4) to the substrate oxygen atom.

The proton-transfer step starting from **16a** involves a free-energy barrier of 8.5 kcal mol^{-1} (see **TS[16a–17b]**‡, Figure 11) and is exergonic by close to 16 kcal mol^{-1}. The most stable product of the proton transfers (**17a**, Figure 12) is –45.7 kcal mol^{-1} more stable than the starting structure of the present study, **13a** (Figure 3). Furthermore, the imidazole ring of His285 is rotated "upright" by ca. 90° compared with the "in-plane" conformation seen for this residue in **16**. In the "upright" conformation in **17**, Glu286 is oriented so that the proton that was transferred to this residue from the substrate in the tautomerization step now forms a hydrogen bond with Wat4. Glu286 also forms a hydrogen bond with the cofactor, which, in turn, forms hydrogen bonds with Glu330 and His290.

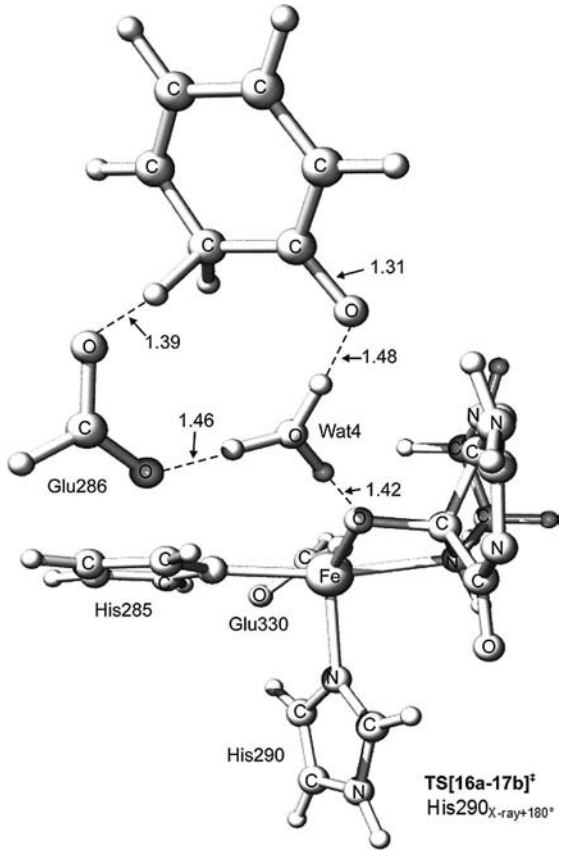

Figure 11. Geometry-optimized transition state for proton transfers from the substrate to Glu286 and from Wat4 to the substrate. Distances are given in Å.

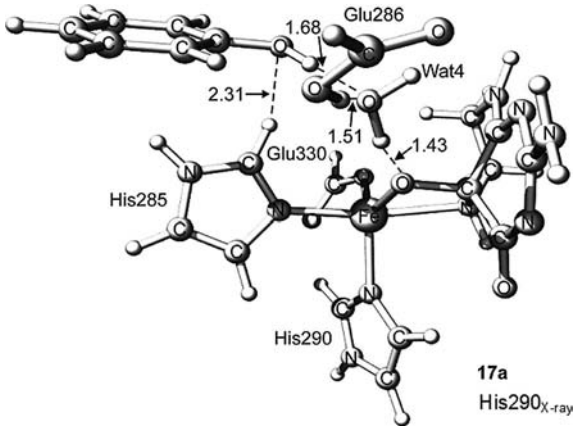

Figure 12. Geometry-optimized structure after tautomerization where the oxidized amino acid is now in the phenol form. Distances are given in Å.

Before protonation of the oxidized cofactor, His285 rotates down again to an "in-plane" conformation, albeit in an orientation ca. 180° relative to that of **16**. This rotation requires only insignificant activation ($\Delta G^{\ddagger}$ = 1.2 kcal mol^{-1}, **TS[17a–18b]**‡ in Figure 13) and results in structure **18b** (in the Supporting Information) which is slightly less stable than **18a** (Figure 14). The rotation of His285 allows for a tight hydrogen-bonding pattern, facilitating the subsequent protonation of the oxidized cofactor. In particular, the "upright" His285 conformation leads to structures in which the phenol is farther removed from Wat4 and the iron atom, resulting in an energetically less favorable proton transfer.

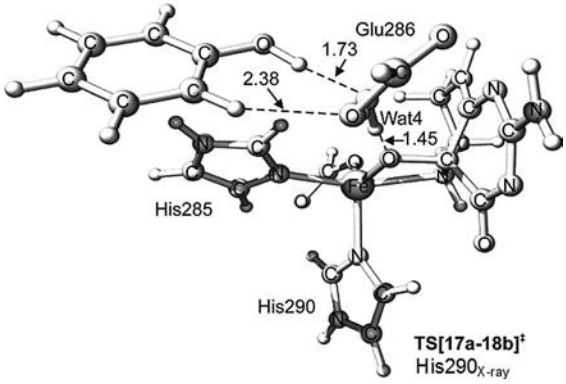

Figure 13. Geometry-optimized transition state for rotation of His285 after protonation of the substrate. Distances are given in Å.

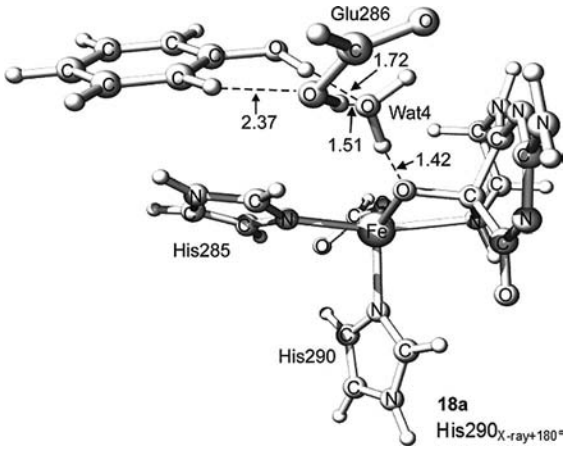

Figure 14. Geometry-optimized structure with His285 rotated. Distances are given in Å.

Protonation of the Oxidized Cofactor

The protonation of the oxidized cofactor is triggered by a small change in the phenol orientation to accommodate hydrogen bonds between the substrate hydroxy group and both Glu286 and Wat4, instead of an interaction with Wat4 only. This rearrangement requires a negligible barrier (3.9 kcal mol^{-1}) (structure **TS[18a–19a]**‡, Figure 15) and hardly affects the binding of the cofactor to the iron atom (structure **19a**, Figure 16).

Rebinding of Water Molecules

To complete the catalytic cycle and regenerate the hexacoordinate iron complex from which the reaction was started (structure **1** in ref.[17]), the iron atom in **19** must undergo dissociation of the oxidized cofactor and coordina-

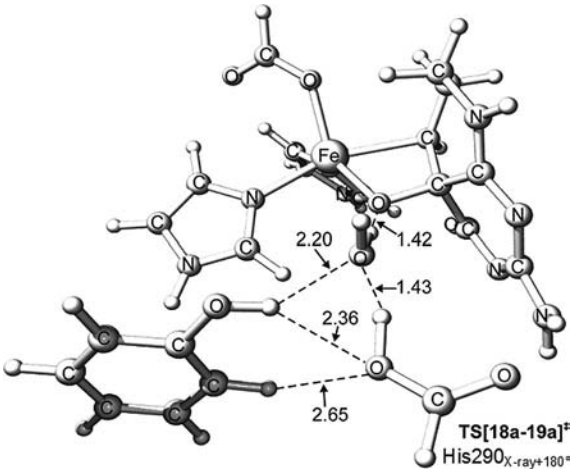

Figure 15. Geometry-optimized transition state for the protonation of the cofactor. Distances are given in Å.

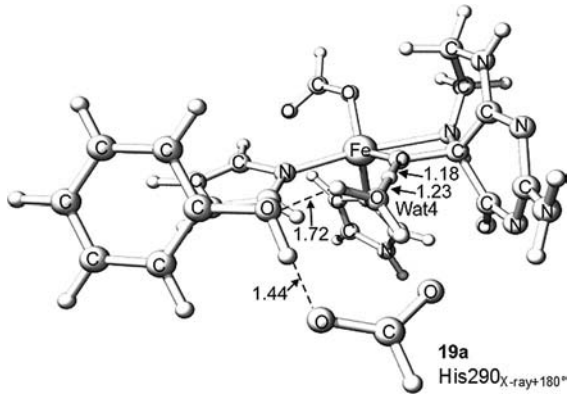

Figure 16. Geometry-optimized structure of the complex featuring the protonated cofactor. Distances are given in Å.

tion of three water molecules. Although the positions of the water molecules in the binary complex involving the reduced cofactor, BH_4, are known from the X-ray crystal structure[14] on which the model in this study was based, the positions in the binary complex with the oxidized cofactor, as well as the order in which these positions should be occupied, are unknown. The calculations show that coordination of the first water molecule in the position of Wat2 in the X-ray crystal structure, a position which is vacant and appears to be accessible in **19**, gives the most stable complex (**20a**, Figure 17) with a bond enthalpy of 7.0 kcal mol^{-1} (enthalpy of reaction **19a** + H_2O → **20a**, ΔH_{tot} = –7.0 kcal mol^{-1}, ΔG_{tot} = 3.3 kcal mol^{-1}). In comparison, the reaction enthalpy for water uptake at the position of Wat1 is higher (ΔH_{tot} = 3.7 kcal mol^{-1}, ΔG_{tot} = 11.4 kcal mol^{-1}), as is the case also for Wat3 (ΔH_{tot} = –2.5 kcal mol^{-1}, ΔG_{tot} = 5.5 kcal mol^{-1}). The oxidized cofactor remains coordinated to the iron atom in all of these structures.

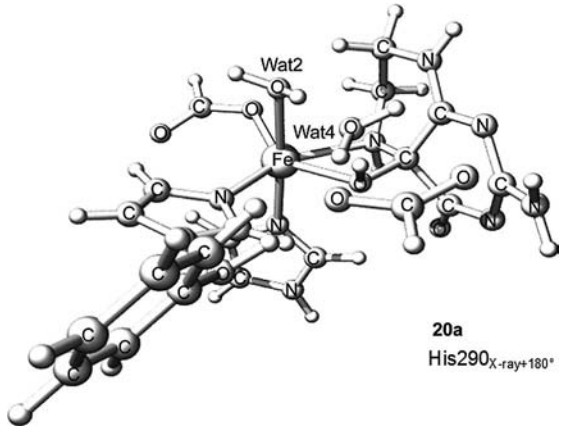

Figure 17. Geometry-optimized structure after binding of a water molecule to the iron atom at the position of Wat2.

Continuing from **20a**, a second water molecule should be coordinated at the position of Wat3 (structure **21a**, Figure 18), which is favorable (enthalpy of reaction **20a** + H_2O → **21a**, ΔH_{tot} = –7.7 kcal mol^{-1}, ΔG_{tot} = 0.0 kcal mol^{-1}) compared with water coordination at position Wat1 (ΔH_{tot} = –0.7 kcal mol^{-1}, ΔG_{tot} = 9.8 kcal mol^{-1}). The Fe–O4 and Fe–N5 bonds are broken upon uptake of the second water molecule, and the cofactor dissociates from the iron atom, resulting in a pentacoordinate iron complex with the oxidized cofactor placed in the second coordination sphere, maintaining strong hydrogen bonds with both Wat2 (1.70 Å) and Wat3 (1.62 Å). It is noteworthy that our calculations show that a feasible reaction is obtained in which the oxidized cofactor only dissociates from the iron atom after completion of the substrate oxidation. Explicit attempts at dissociating the cofactor prior to this point have not been undertaken, though. Nevertheless, the cofactor acts as a bidentate ligand during the complete substrate oxidation and would probably require significant activation in order to be removed. More importantly, removal of the bidentate cofactor would leave the iron complex with an unrealistically low coordination number. The complex would

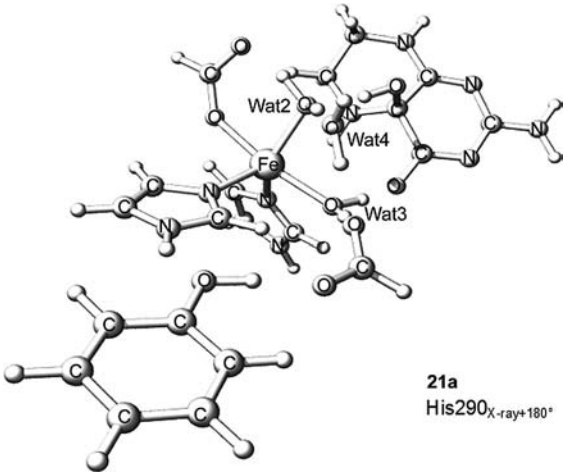

Figure 18. Geometry-optimized structure after binding of the second water molecule to the iron atom in the position of Wat3.

rapidly be saturated by water ligands, with the formation of hydrogen peroxide as the probable result.[45,46] Our calculations thus suggest that the products are released only when both oxidation reactions have been completed.

The coordination of the second water molecule in the position of Wat1 gave a structure in which the cofactor remained coordinated to the iron atom. The higher free energy of the latter structure (by 9.8 kcal mol^{-1}) compared with that of the dissociated cofactor (**21a**) indicates that the cofactor is preferably dissociated from the iron atom during coordination of the second water molecule.

The last water molecule was coordinated to the iron atom at the position of Wat1, with an enthalpy ΔH_{tot} = –9.9 kcal mol^{-1} (ΔG_{tot} = 5.2 kcal mol^{-1}) relative to **21a** (cf. structure **22a**, Figure 19). The hexacoordinate iron complex with three ligating water molecules is now restored and after release of the products a new catalytic cycle can start. The release in free energy when removing the phenol from the second coordination sphere of **22a** is 3.3 kcal mol^{-1}, and the resulting iron complex with the oxidized cofactor (pterin-4a-carbinolamine; see Scheme 2) is 62.4 kcal mol^{-1} more stable than the hexacoordinate complex (**1a**, cf. ref.[17]). The net overall reaction is benzene + O_2 + BH_4 → phenol + **4a**–HO–BH_4, with a corresponding free energy of reaction calculated to be –62.8 kcal mol^{-1}. The close agreement between the result for the catalyzed and the uncatalyzed reaction is gratifying. The slightly lower exergonicity of the former is expected since the oxidation of the cofactor reduces its affinity towards the active-site–metal complex.[47,48] It should be noted that the same computational strategy (see the Computational Details section) for obtaining thermodynamic functions has been followed in all calculations. This implies that the reference state (the asymptote for the calculation of relative free energies) for molecules taken up or released from our enzyme cluster model, including water molecules rebound to the iron atom to conclude the catalytic cycle, is that of an unspecified site in the protein environment, i.e. a single molecule experiencing average polarization effects from the surrounding protein.

The above considerations concerning rebinding of water molecules have only been based on thermodynamics. The highest barrier to water binding should be expected for the sterically most congested complex, i.e. for coordination to **21a**, where it would represent the rate-determining step of the catalyst regeneration part of the reaction, i.e. the part following the tautomerization. However, an analogous transition state for dissociation of a water ligand from the hexacoordinate iron starting complex **1** has been located. This transition state represents a barrier amounting to 4.4 kcal mol^{-1} from **1**, suggesting that a barrier of similar magnitude should be operative for the corresponding water dissociation from **22a**. Assuming that water binding and dissociation follows the same path in these complexes, the effective barrier in the catalyst regeneration part of the reaction is estimated to be 13.1 kcal mol^{-1}, i.e. similar to that for (Fe)O–C(benzene) formation and slightly lower than the rate-determining barrier energy for the overall catalytic reaction (13.9 kcal mol^{-1}), pertaining to the formation of the

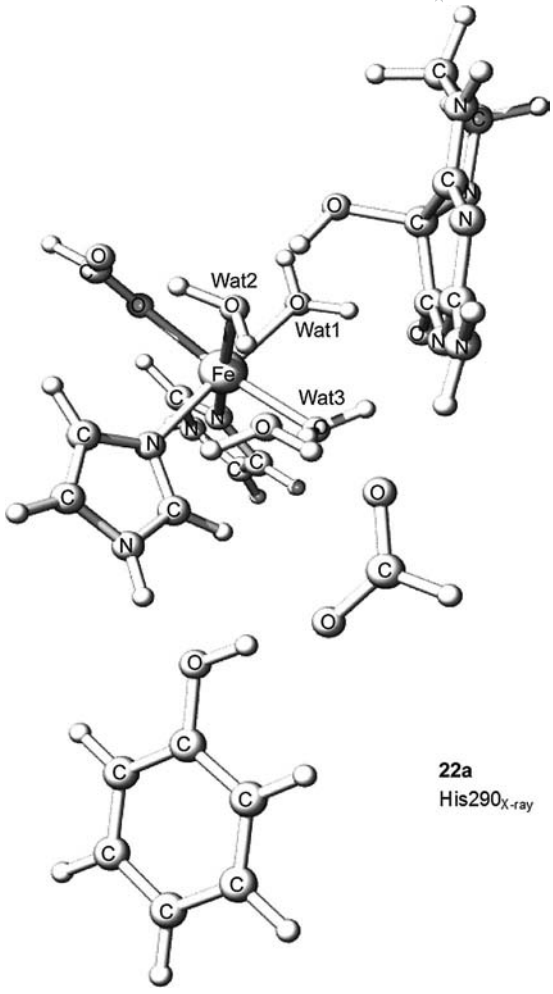

Figure 19. Geometry-optimized structure with the last water molecule bound to the iron atom at the position of Wat1.

Fe^{IV}=O hydroxylating species.[24] The most stable intermediate in this part of the reaction (**18**) is located ca. 9 kcal mol^{-1} below the final point (**22**) in free energy. The effective rate-limiting step used in our previous study[24] was calculated relative to an intermediate (**3a**), 6.9 kcal mol below the starting point (**1a**).[17] From the second catalytic cycle and onwards the effective rate-limiting step should be calculated relative to **18**, resulting in an energy barrier (15.8 kcal mol^{-1}) that is in even better agreement with the experimental data (15.6 kcal mol^{-1}).[23,49]

Conclusions

Using a cluster model based on the X-ray crystal structure of the catalytic domain of hPAH in a binary complex with the cofactor (hPAH–Fe^{II}–BH_4), we have followed, by means of DFT calculations, the oxygen insertion mechanism for the hydroxylation of benzene (as a model of the aromatic amino acid substrate) to phenol as mediated by the Fe^{IV}=O intermediate. The water-free gas-phase cluster model that constitutes the starting point in this study was arrived at in previous studies of water–ligand dissociation

from the hexacoordinate iron complex of the hPAH–Fe^{II}–BH_4 enzyme resting state[17] and the subsequent formation of the high-valent hydroxylating intermediate.[24] This Fe^{IV}=O cluster model contains no iron-coordinating water molecules, has the pterin cofactor placed in the first coordination sphere of the metal atom, and differs substantially from the cluster model applied in previous studies.[35,36]

In the present investigation of substrate hydroxylation, we find that the first step, the electrophilic aromatic addition [i.e. the formation of the (Fe)O–C(benzene) bond], is associated with an activation free energy of 12.6 kcal mol^{-1}. In comparison with the corresponding calculations for initial parts of the catalytic cycle,[24] this barrier is ca. 1 kcal mol^{-1} lower than the overall effective energy barrier for the formation of the Fe^{IV}=O species (13.9 kcal mol^{-1}). These calculated barrier heights are in excellent agreement with the fact that, in most cases, formation of the hydroxylating intermediate appears to represent the rate-limiting step, although there are also examples where oxygen insertion into the amino acid substrate takes on a partial or complete rate-determining role,[3,27] indicating that the two barriers are intrinsically of comparable magnitudes and that their relative order may be modified by the exact choice of enzyme, substrate, and cofactor.

The final steps of the substrate hydroxylation, the 1,2-hydride shift (NIH shift) to generate the dienone and the tautomerization to reach the phenol form, are both associated with comparably lower barriers (10.0 kcal mol^{-1} and 8.5 kcal mol^{-1}, respectively), and the subsequent protonation of the oxidized iron-bound cofactor to give the expected pterin-4a-carbinolamine product is facile ($\Delta G^{\ddagger}_{tot}$ = 3.9 kcal mol^{-1}).

For the first time in a molecular-level computational study of the AAH mechanism, completion of the catalytic cycle and regeneration of the catalyst are achieved. The regeneration of the enzyme resting state involves rebinding of water molecules and decoordination of the pterin-4a-carbinolamine and is thermodynamically facile. Calculations of water dissociation and cofactor coordination for the same model complex[17] suggest that the associated barriers should be comparable to that of (Fe)O–C(benzene) bond formation, i.e. somewhat lower than that of the overall rate-determining step. Another difference from previous computational studies[35,36] is that our calculations predict that no product is released before the oxidation of both the substrate and the cofactor has been completed, and this is in agreement with the observation that no product is released prior to the binding of all substrates.[32]

Computational Details

All calculations were performed using Becke's three-parameter hybrid-generalized gradient approximation (GGA) density functional (termed B3LYP)[50,51] as implemented in the Gaussian 03 suite of programs.[52] All minima and transition states were fully optimized and characterized using algorithms involving analytical first and second derivatives of the energy. Translational, rotational, and vibrational partition functions to give thermal corrections (ΔH_{gas} and ΔG_{gas}) were computed from the harmonic frequencies at 298 K within the ideal-gas, rigid-rotor, and harmonic-oscillator approximations according to standard procedures. For the geometry optimizations and the vibrational analyses the basis sets used (termed LANL2DZ) are described as follows: For iron, the Hay and Wadt effective core potential (ECP)[53] was used for the 10 inner electrons in the 1s, 2s, and 2p shells. The outer electrons in the 3s, 3p, 3d, and 4s shells were described by the Hay and Wadt (5s,5p,5d) primitive basis set[53] contracted to [3s,3p,2d]. Standard Dunning and Hay valence double-ζ basis sets[54] were used to describe the hydrogen, carbon, nitrogen, and oxygen atoms.

Single-point (SP) energy calculations, giving energies termed $E_{SP,gas}$, were performed on the optimized geometries using the B3LYP functional in combination with basis sets that were improved compared with those used in the geometry optimizations. For iron, the Hay and Wadt (5s,5p,5d) primitive basis set[53] was contracted to [4s,4p,3d]. For hydrogen, the Dunning and Hay double-ζ basis set[54] was extended with single sets of diffuse s and polarization p functions, resulting in a (5s,1p) primitive basis set contracted to [3s,1p]. For carbon, nitrogen, and oxygen, the Dunning and Hay standard valence double-ζ basis sets[54] were extended with single sets of diffuse p and polarization d functions, resulting in (9s,6p,1d) primitive basis sets that were contracted to [3s,3d,1d].

A polarized continuum model (PCM)[55] was used in the final SP calculations to model the polarization effects from the surrounding protein. The resulting solvation energies are termed ΔE_{solv}. A dielectric constant (ε) of four was used in the calculations in which the temperature was set to 298 K. Only electrostatic terms were included. The Bondi set of atomic radii[56] was used to construct the cavity. Finally, standard density functionals based on the GGA approximation, including the currently applied B3LYP functional, do not account for noncovalent dispersion-type interactions. We have thus included an empirical term for long-range dispersion, leading to corrections termed ΔE_{disp}, in our final energy estimates, which thus can be termed "B3LYP-D".[57] In general, GGA-based methods including such an empirical term (i.e. DFT-D) show substantial improvement in accuracy over the parent DFT functionals, and in particular reduce the systematic tendency towards underbinding.[57–60]

The three water molecules that are rebound to the iron atom at the end of the catalytic cycle were treated as originating from an unspecified site in the protein environment. The energy of such water molecules not coordinated to the iron atom was calculated assuming a single, gas-phase water molecule experiencing average polarization effects from the surrounding protein, i.e. the general strategy described above. This strategy does not account for the specific interactions that would exist between such a water molecule and hydrophilic amino acid residues in the protein. However, at the same time this approach overestimates the entropy of the single water molecule, presumably leading to substantial error cancellation. Alternatively, the water molecules could have been treated as originating from bulk water.[61] Whereas using bulk water as a reference state should lead to stabilization of this state since condensation of water is spontaneous (by 2 kcal mol^{-1})[62] at 25 °C, a 5.6 kcal mol^{-1} destabilization due to the removal of the average polarization effect from the protein environment (the PCM treatment described above) also has to be factored in. The result would be a modest overall destabilization (amounting to 3.6 kcal mol^{-1}) of the reference state for each water molecule compared with the current in-protein asymptote. In such a scenario, the more favorable water coordination to the iron atom would flatten the free energy surface of the water dissociations and associations at the initial and final

stages of the overall catalytic reaction, respectively. The rate-determining transition state would still be that of the one-electron transfer from the cofactor to dioxygen leading up to the formation of the Fe^{IV}=O hydroxylating species. However, because of the less favorable initial water dissociation, the lowest-lying intermediate (**2**) from which the overall effective barrier would have to be calculated would be less stable (1.7 kcal mol^{-1} below the asymptote) than with the current in-protein water reference state, leading to a lower calculated energy barrier (8.7 kcal mol^{-1}). In other words, the reference states for water molecules and substrates influence the absolute barrier heights. The mechanism itself, however, is not affected.

Natural charges and natural spin densities for the iron atom, the oxygen atoms in dioxygen, and the cofactor BH_4, as well as the Wiberg bond index for Fe–Oa, Oa–Ob, and Ob–C4a were obtained using natural population analysis (NPA)[63] as implemented in the natural-bond orbital (NBO) program.[64]

The above-described energy contributions, the relative energies, and enthalpies reported in this study are defined as $\Delta G_{SP,gas} = \Delta E_{SP,gas} + \Delta G_{gas}$, $\Delta G_{tot} = \Delta E_{SP,gas} + \Delta E_{solv} + \Delta E_{disp} + \Delta G_{gas}$, $\Delta G_{tot\text{-}disp} = \Delta E_{SP,gas} + \Delta E_{solv} + \Delta G_{gas}$, and $\Delta H_{tot} = \Delta E_{SP,gas} + \Delta E_{solv} + \Delta E_{disp} + \Delta H_{gas}$. Unless otherwise stated the free energies are given as ΔG_{tot}.

Supporting Information (see footnote on the first page of this article): Alignment of **12a** and **13a** (Figure S1); total energies, thermochemical, dispersion, and solvent corrections (Table S1), relative energies and enthalpies (Table S2), natural charges (Table S3), Wiberg bond indices (Table S4), spin populations (Table S5), and Cartesian coordinates calculated for the stationary points and conformations located along the reaction path.

Acknowledgments

University of Bergen is acknowledged for financial support through the Nanoscience program. The Norwegian Research Council is acknowledged for CPU resources granted through the NOTUR supercomputing program. We are grateful to Giovanni Occhipinti for helpful discussions.

[1] M. M. Abu-Omar, A. Loaiza, N. Hontzeas, *Chem. Rev.* **2005**, *105*, 2227–2252.
[2] P. F. Fitzpatrick, *Annu. Rev. Biochem.* **1999**, *68*, 355–381.
[3] P. F. Fitzpatrick, *Biochemistry* **2003**, *42*, 14083–14091.
[4] T. Flatmark, R. C. Stevens, *Chem. Rev.* **1999**, *99*, 2137–2160.
[5] T. J. Kappock, J. P. Caradonna, *Chem. Rev.* **1996**, *96*, 2659–2756.
[6] K. Teigen, J. A. McKinney, J. Haavik, A. Martinez, *Curr. Med. Chem.* **2007**, *14*, 455–467.
[7] D. J. Walther, M. Bader, *Biochem. Pharmacol.* **2003**, *66*, 1673–1680.
[8] D. B. Fisher, S. Kaufman, R. Kirkwood, *J. Biol. Chem.* **1972**, *247*, 5161–5167.
[9] D. W. Gottschall, R. F. Dietrich, S. J. Benkovic, R. Shiman, *J. Biol. Chem.* **1982**, *257*, 845–849.
[10] G. R. Moran, S. C. Daubner, P. F. Fitzpatrick, *J. Biol. Chem.* **1998**, *273*, 12259–12266.
[11] B. Thony, G. Auerbach, N. Blau, *Biochem. J.* **2000**, *347*, 1–16.
[12] T. A. Dix, G. E. Bollag, P. L. Domanico, S. J. Benkovic, *Biochemistry* **1985**, *24*, 2955–2958.
[13] H. U. Siegmund, S. Kaufman, *J. Biol. Chem.* **1991**, *266*, 2903–2910.
[14] O. A. Andersen, T. Flatmark, E. Hough, *J. Mol. Biol.* **2001**, *314*, 279–291.
[15] K. E. Goodwill, C. Sabatier, R. C. Stevens, *Biochemistry* **1998**, *37*, 13437–13445.
[16] L. Wang, H. Erlandsen, J. Haavik, P. M. Knappskog, R. C. Stevens, *Biochemistry* **2002**, *41*, 12569–12574.
[17] E. Olsson, A. Martinez, K. Teigen, V. R. Jensen, *Eur. J. Inorg. Chem.* **2010**, 351–356.
[18] E. I. Solomon, T. C. Brunold, M. I. Davis, J. N. Kemsley, S. K. Lee, N. Lehnert, F. Neese, A. J. Skulan, Y. S. Yang, J. Zhou, *Chem. Rev.* **2000**, *100*, 235–349.
[19] M. Costas, M. P. Mehn, M. P. Jensen, L. Que, *Chem. Rev.* **2004**, *104*, 939–986.
[20] T. A. Dix, S. J. Benkovic, *Biochemistry* **1985**, *24*, 5839–5846.
[21] A. L. Feig, S. J. Lippard, *Chem. Rev.* **1994**, *94*, 759–805.
[22] B. E. Eser, E. W. Barr, P. A. Frantorn, L. Saleh, J. M. Bollinger, C. Krebs, P. F. Fitzpatrick, *J. Am. Chem. Soc.* **2007**, *129*, 11334–11335.
[23] A. Bassan, M. R. A. Blomberg, P. E. M. Siegbahn, *Chem. Eur. J.* **2003**, *9*, 106–115.
[24] E. Olsson, A. Martinez, K. Teigen, V. R. Jensen, *Chem. Eur. J.* **2011**, *17*, 3746–3758.
[25] W. A. Francisco, G. C. Tian, P. F. Fitzpatrick, J. P. Klinman, *J. Am. Chem. Soc.* **1998**, *120*, 4057–4062.
[26] P. F. Fitzpatrick, *Biochemistry* **1991**, *30*, 6386–6391.
[27] G. R. Moran, R. S. Phillips, P. F. Fitzpatrick, *Biochemistry* **1999**, *38*, 16283–16289.
[28] G. Guroff, J. W. Daly, D. M. Jerina, J. Renson, B. Witkop, S. Udenfrie, *Science* **1967**, *157*, 1524.
[29] P. F. Fitzpatrick, *J. Am. Chem. Soc.* **1994**, *116*, 1133–1134.
[30] A. J. Panay, P. F. Fitzpatrick, *Biochemistry* **2008**, *47*, 11118–11124.
[31] J. A. Blair, A. J. Pearson, *J. Chem. Soc. Perkin Trans. 2* **1975**, 245–249.
[32] T. J. Kappock, P. C. Harkins, S. Friedenberg, J. P. Caradonna, *J. Biol. Chem.* **1995**, *270*, 30532–30544.
[33] A. Volner, J. Zoidakis, M. M. Abu-Omar, *J. Biol. Inorg. Chem.* **2003**, *8*, 121–128.
[34] P. J. Hillas, P. F. Fitzpatrick, *Biochemistry* **1996**, *35*, 6969–6975.
[35] A. Bassan, M. R. A. Blomberg, P. E. M. Siegbahn, *Chem. Eur. J.* **2003**, *9*, 4055–4067.
[36] Y. Shiota, K. Yoshizawa, *J. Phys. Chem. B* **2004**, *108*, 17226–17237.
[37] M. R. Jackson, R. Beahm, S. Duvvuru, C. Narasimhan, J. Wu, H. N. Wang, V. M. Philip, R. J. Hinde, E. E. Howell, *J. Phys. Chem. B* **2007**, *111*, 8242–8249.
[38] D. J. Heisterberg, *Quatfit*, unpublished results.
[39] O. A. Andersen, T. Flatmark, E. Hough, *J. Mol. Biol.* **2002**, *320*, 1095–1108.
[40] O. A. Andersen, A. J. Stokka, T. Flatmark, E. Hough, *J. Mol. Biol.* **2003**, *333*, 747–757.
[41] A. Y. Han, A. Q. Lee, M. M. Abu-Omar, *Inorg. Chem.* **2006**, *45*, 4277–4283.
[42] K. Teigen, N. A. Frøystein, A. Martinez, *J. Mol. Biol.* **1999**, *294*, 807–823.
[43] S. Olafsdottir, A. Martinez, *J. Biol. Chem.* **1999**, *274*, 6280–6284.
[44] W. D. Lehmann, H. C. Heinrich, *Arch. Biochem. Biophys.* **1986**, *250*, 180–185.
[45] P. J. Loida, S. G. Sligar, *Biochemistry* **1993**, *32*, 11530–11538.
[46] T. I. Oprea, G. Hummer, A. E. Garcia, *Proc. Natl. Acad. Sci. USA* **1997**, *94*, 2133–2138.
[47] S. W. Bailey, J. E. Ayling, *Biochemistry* **1983**, *22*, 1790–1798.
[48] J. Haavik, A. P. Døskeland, T. Flatmark, *Eur. J. Biochem.* **1986**, *160*, 1–8.
[49] M. A. Hill, J. J. A. Marota, R. Shiman, *J. Biol. Chem.* **1988**, *263*, 5646–5655.
[50] A. D. Becke, *J. Chem. Phys.* **1993**, *98*, 5648–5652.
[51] P. J. Stephens, F. J. Devlin, C. F. Chabalowski, M. J. Frisch, *J. Phys. Chem.* **1994**, *98*, 11623–11627.
[52] M. J. Frisch, G. W. Trucks, H. B. Schlegel, G. E. Scuseria, M. A. Robb, J. R. Cheeseman, J. A Montgomery Jr., T. Vreven, K. N. Kudin, J. C. Burant, J. M. Milliam, S. S. Iyengar, J. Tomasi, V. Barone, B. Mennucci, M. Cossi, G. Scalmani, N. Rega,

G. A. Peterson, H. Nakatsuji, M. Hada, M. Ehara, K. Toyota, R. Fukuda, J. Hasegawa, M. Ishida, T. Nakajima, Y. Honda, O. Kitao, H. Nakai, M. Klene, X. Li, J. E. Know, H. P. Hratchian, J. B. Cross, V. Bakken, C. Adamo, J. Jaramillo, R. Gomperts, R. E. Stratmann, O. Yazyev, A. J. Austin, R. Cammi, C. Pomelli, J. W. Ochterski, P. Y. Ayala, K. Morokuma, G. A. Voth, P. Salvador, J. J. Dannenberg, V. G. Zakrzewski, S. Dapprich, A. D. Daniels, M. C. Strain, O. Farkas, D. K. Malick, A. D. Rabuck, K. Raghavachari, J. B. Foresman, J. V. Ortiz, Q. Cui, A. G. Baboul, S. Clifford, J. Cioslowski, B. B. Stefanov, G. Liu, A. Liashenko, P. Piskorz, I. Komaromi, R. L. Martin, D. J. Fox, T. Keith, M. A. Al-Laham, C. Y. Peng, A. Nanayakkara, M. Challacombe, P. M. W. Gill, B. Johnson, W. Chen, M. W. Wong, C. Gonzalez, J. A. Pople, *Gaussian 03, Revision E.01*, Gaussian, Inc., Wallingford, CT, **2004**.

[53] P. J. Hay, W. R. Wadt, *J. Chem. Phys.* **1985**, *82*, 299–310.

[54] T. H. Dunning, P. J. Hay in *Methods of Electronic Structure Theory*, vol. 2 (Ed.:H. F. Schaefer), Plenum Press, New York, **1977**, pp. 1–27.

[55] J. Tomasi, M. Persico, *Chem. Rev.* **1994**, *94*, 2027–2094.

[56] A. Bondi, *J. Phys. Chem.* **1964**, *68*, 441–451.

[57] S. Grimme, *J. Comput. Chem.* **2006**, *27*, 1787–1799.

[58] S. Grimme, J. Antony, T. Schwabe, C. Muck-Lichtenfeld, *Org. Biomol. Chem.* **2007**, *5*, 741–758.

[59] T. Schwabe, S. Grimme, *Phys. Chem. Chem. Phys.* **2007**, *9*, 3397–3406.

[60] T. Schwabe, S. Grimme, *Acc. Chem. Res.* **2008**, *41*, 569–579.

[61] P. E. M. Siegbahn, M. R. A. Blomberg, *J. Phys. Chem. A* **2008**, *112*, 12772–12780.

[62] G. Aylward, T. Findlay, *SI Chemical Data*, 4th ed., John Wiley & Sons, Brisbane, **1998**.

[63] A. E. Reed, R. B. Weinstock, F. Weinhold, *J. Chem. Phys.* **1985**, *83*, 735–746.

[64] E. D. Glendening, J. K. Badenhoop, A. E. Reed, J. E. Carpenter, J. A. Bohmann, C. M. Morales, F. Weinhold, *NBO 5.0*, Theoretical Chemistry Institute, University of Wisconsin, Wisconsin, **2001**.

Received: November 21, 2010
Published Online: May 2, 2011

